



## Flood susceptibility mapping in Kali River Basin, Southern India: A GIS-based analytical hierarchy process modelling

Ananda Krishnan <sup>a</sup>, S.G. Dhanil Dev <sup>a,\*</sup>, S. Arjun <sup>a,b</sup>, V. Deepchand <sup>a</sup>, Yogendra Singh <sup>b</sup>, E. Shaji <sup>a</sup>, P.K. Krishnaprasad <sup>a</sup>

<sup>a</sup> Department of Geology, University of Kerala, Kariavattom Campus, Trivandrum 695581, India

<sup>b</sup> Seismotectonic Department, National Institute of Rock Mechanics, Bangalore, 560070

### ARTICLE INFO

**Keywords:**  
 Uttara Kannada  
 Flood Risk Assessment  
 Multi-Criteria Decision Analysis (MCDA)  
 Remote Sensing  
 Receiver Operating Characteristic (ROC) Curve

### ABSTRACT

Across the globe, floods are always a matter of concern for everyone due to the uncertainty of their occurrence and place. Though their prediction is still in the progress stage, there are enough methods available to identify the areas that have the potential to experience any specific kind of hazard. The present study is focused on an area located in the Uttara Kannada district of Karnataka and the South Goa district in Goa, which experienced a natural hazard for the first time in the form of the Kali River flood in 2019. The study aims to develop flood susceptibility maps for selected subbasins of the Kali River using integrated remote sensing techniques with the analytical hierarchy process system. Detailed analyses of numerous causative factors, i.e., elevation, slope, distance from the river, precipitation, flow accumulation, stream density, soil types, water ratio index, land use land cover, topographic wetness index, and stream power index, were carried out. The result shows that the area can be categorized into five zones ranging from very low to very high susceptibility to flooding. The prevalence of flooding in the study area can be attributed to increased sediment deposition, anthropogenic disturbances, land use and land cover patterns, gentle slopes, elevated soil moisture levels, reduced stream capacity, and limited soil infiltration capacity. The accuracy of the result was assessed using the receiver operating characteristic (ROC) method and confirmed the predictive capability of the generated map. Approximately 30 % of the study area falls within the highly susceptible zone. The outcome of the study provides valuable insights for urban planners and policymakers, assisting them in formulating strategies to mitigate the impact of future flood hazards and minimize the damages, particularly in southwest coast India.

### Introduction

In the intricate tapestry of Earth's natural phenomena, few occurrences are as awe-inspiring and devastating as floods. Floods are natural disasters that often cause severe damage to property and loss of life (Merkuryeva et al., 2015; Vilasan and Kapse, 2022). This state can be caused by various hydrological phenomena, including high tides, precipitation, high groundwater levels, and high river flows (Acreman and Holden, 2013). They occur when an overwhelming amount of water submerges ordinarily dry land, often due to heavy rainfall, snowmelt, storm surges, or the failure of water containment structures such as dams and levees (Acreman and Holden, 2013). This natural occurrence, driven by a combination of atmospheric conditions and geographic factors, encompasses a spectrum of intensities, from gentle inundations that replenish arid regions to cataclysmic deluges that wreak havoc on

communities.

Floods, both slow and rapid-onset, affect regions globally, primarily due to excessive rainfall from monsoons, hurricanes, or prolonged storms. Factors like climate changes and land use shifts (Charlton et al., 2006; Ali et al., 2020) exacerbate these events. Poor drainage in urban areas with impermeable surfaces increases flood risk, as does deforestation and construction in floodplains. Climate change, through rising temperatures and extreme weather patterns, heightens flood frequency and intensity (Panagoulia and Dimou, 1997; Rojas et al., 2012; Das, 2018; Rajkhowa and Sarma, 2021). The frequency and intensity of extreme weather events, including heavy rainfall and flooding, are expected to increase due to global warming, particularly in regions like the Kali River Basin, where monsoon rains and anthropogenic activities such as deforestation and urbanization significantly increase flood vulnerability (Rajkhowa and Sarma, 2021).

\* Correspondence to: Department of Geology, University of Kerala, Kariavattom Campus, Trivandrum - 695 581, Kerala, India.

E-mail address: [dhanildev@keralauniversity.ac.in](mailto:dhanildev@keralauniversity.ac.in) (S.G.D. Dev).

Floods devastate human life and property, causing fatalities, displacements, and destruction of homes, infrastructure, and agriculture (Petersen, 2001; Smiley and Hambati, 2019). Survivors face waterborne diseases, food shortages, disrupted services, and inadequate temporary housing (Allaire, 2018). Environmentally, floods cause soil erosion, biodiversity loss, and water contamination with sediments and pollutants, harming aquatic ecosystems and reducing the effectiveness of natural flood deterrents.

Approximately 100 million individuals across the globe were affected by disastrous floods from 2000 to 2008 (Opolot, 2013; Das, 2018). Such occurrences are frequently observed in developing countries characterized by substantial urbanization and societal expansion along riverbanks. In these regions, the process of deforestation to facilitate settlements and altering river trajectories often serves as the impetus for flood events (Bronstert, 2003; Christensen and Christensen, 2003; Das, 2018). Flooding is a frequently occurring natural hazard in India (Vilasan and Kapse, 2022). Due to this, the country has been positioned third in the world risk index for 2023. India is prone to flooding primarily due to its southwest monsoon climate, topography, and river systems. About 40 million hectares, around 12% of Indian land, are susceptible to flooding. After Bangladesh, India is a nation with the worst effects worldwide (Panda and Sahoo, 2015).

In recent years, remote sensing and geographic information systems have emerged as transformative tools in hazard management and geo-spatial mapping through multi-criteria decision models (Das et al., 2017). These methodologies find applications across various geohazards, encompassing floods, droughts, forest fires, and landslides. Over the past two decades, the adoption of these techniques has gained significant traction among researchers. Diverse methodologies have been developed to assess flood vulnerability, including the analytical hierarchy process (Dou et al., 2018; Vilasan and Kapse, 2022), fuzzy logic in combination with genetic algorithms (Nourani et al., 2014; Hong et al., 2018), variable fuzzy theory (Guo et al., 2014), among several others (Das, 2018). The integration of GIS and remote sensing technologies has revolutionized flood risk assessment, allowing for the incorporation of multiple factors such as topography, hydrology, and land use changes (Tehrany et al., 2014; Kazakis et al., 2015). The role of land use and land cover (LULC) changes, particularly urbanization, has been widely documented to increase surface runoff and reduce infiltration rates, leading to higher flood risks (Gregory et al., 2006; Gigović et al., 2017).

The Analytical Hierarchy Process (AHP) is a simple and structured technique for analyzing complex decisions, based on mathematics and psychology. It can handle a broad range of criteria and sub-criteria, accommodating various dimensions of flood vulnerability (Karpouza et al., 2023). This flexibility is advantageous over traditional overlay methods, which might be limited in handling complex, multi-faceted issues with multiple interacting layers. AHP is also able to delineate areas susceptible to flooding with minimal or no previous flood data (inventory data) and still provides very promising results. In contrast, machine learning studies often struggle to achieve similar accuracy without extensive historical flood data, as they heavily rely on large datasets to train their models. This makes AHP particularly valuable in regions where historical flood data is scarce or incomplete, allowing for effective flood risk assessment and management based on expert judgment and multi-criteria analysis.

However, AHP relies on expert judgments to assign weights to various criteria, potentially leading to biased outcomes and the process of pairwise comparisons can become cumbersome and time-consuming, especially when dealing with a large number of criteria and alternatives. This complexity can increase the likelihood of inconsistencies in judgments, which might affect the reliability of the results.

The 2019 flood in Karwar taluk of the Uttara Kannada district substantially destroyed infrastructure and property and caused loss of life (Krishnan, 2024). Numerous villages within Karwar taluk encountered waterborne illnesses and grappled with shortages of necessities, food,

and suitable living conditions. In response, approximately 5000 individuals from these villages were relocated to rehabilitation centres in Karwar and adjacent villages. The Indian Navy's diving teams (Indian Navy, 2019, August 07) and boats were crucial in evacuating people to safer locales, particularly in villages neighbouring the Kadra Dam (Thakkar, 2019).

The primary aim of this study is to identify the range of factors contributing to flood incidents and delineate areas within the study region particularly susceptible to flooding. This objective is achieved through the integration of remote sensing data and geographic information systems (GIS), employing the analytical hierarchy process (AHP) methodology. By systematically evaluating factors such as topography, rainfall patterns, land use, soil type, and drainage density, the study provides a comprehensive assessment of flood vulnerability. Additionally, the study seeks to develop and propose mitigation strategies to address the identified flood vulnerabilities, enhancing the region's resilience to future flood events.

## Study area

The study is focused on the subbasins of Kali River, which encompasses parts of the Uttara Kannada district in Karnataka and the South Goa district in Goa (Fig. 1). The investigation area spans from  $15^{\circ} 4' 4.10''$  N to  $14^{\circ} 45' 41.52''$  N latitudes and  $74^{\circ} 5' 14.66''$  E to  $74^{\circ} 41' 54.65''$  E longitudes, covering a total area of  $1175.45\text{ km}^2$ . The topography of this region exhibits diverse elevations, ranging from 0 to 901 m above mean sea level (MSL). The Kali River courses run through the study area, hosting two hydroelectric dams and reservoirs. The landscape is characterised by distinct low-lying hills interspersed with elevated formations. The hydrological network predominantly comprises streams originating from the steep western ghats escarpment, with the highest stream order being seven (Krishnan, 2024). These waterways flow westwards and eventually debouches into the Arabian Sea. A considerable portion of the study zone is enveloped by dense vegetation. The climatic narrative highlights a substantial influx of rainfall during the southwest monsoon, from mid-June until late September, contributing to an annual average rainfall of 3841 mm. This orographic precipitation pattern accentuates the region's vulnerability to flooding in low-lying areas, highlighting the intricate interplay between topography and hydrology (Krishnan, 2024).

## The unprecedented situation

On August 6, 2019, the Karwar taluk of Uttara Kannada district experienced a severe flood event. This flooding was primarily induced by continuous and intense precipitation in the Western Ghats region, leading to the overflow of several rivers, including the Kali River and its tributaries. The inundation affected multiple villages within the Uttara Kannada district, including Kadra, Mallapur, Kaiga township (Fig. 2a and b), Hanakon, Kharge Jooga Island, Kinnar, Siddar, and Vailwada. These areas experienced significant waterlogging, resulting in extensive structural damage (Fig. 2d and e) and disruption to road networks. In response to rising water levels and the imminent threat of landslides (The New Indian Express, 2019), authorities-initiated evacuation procedures to relocate residents to safer areas. Several relief camps were established to provide shelter and essential supplies to displaced individuals. The flooding caused substantial damage to roads, bridges, and other infrastructure, severely disrupting local transportation (Fig. 2c) and communication systems.

The agricultural sector was also significantly affected, with extensive farmland submersion and crop damage, directly impacting the livelihoods of the local population. Additionally, the floods resulted in fatalities and injuries among livestock in the vicinity of the Kali River (Thakkar, 2019). Search and rescue operations (Fig. 2f) were conducted by the National Disaster Response Force (NDRF) and other agencies (Indian Navy, 2019, August 07), providing crucial assistance during the

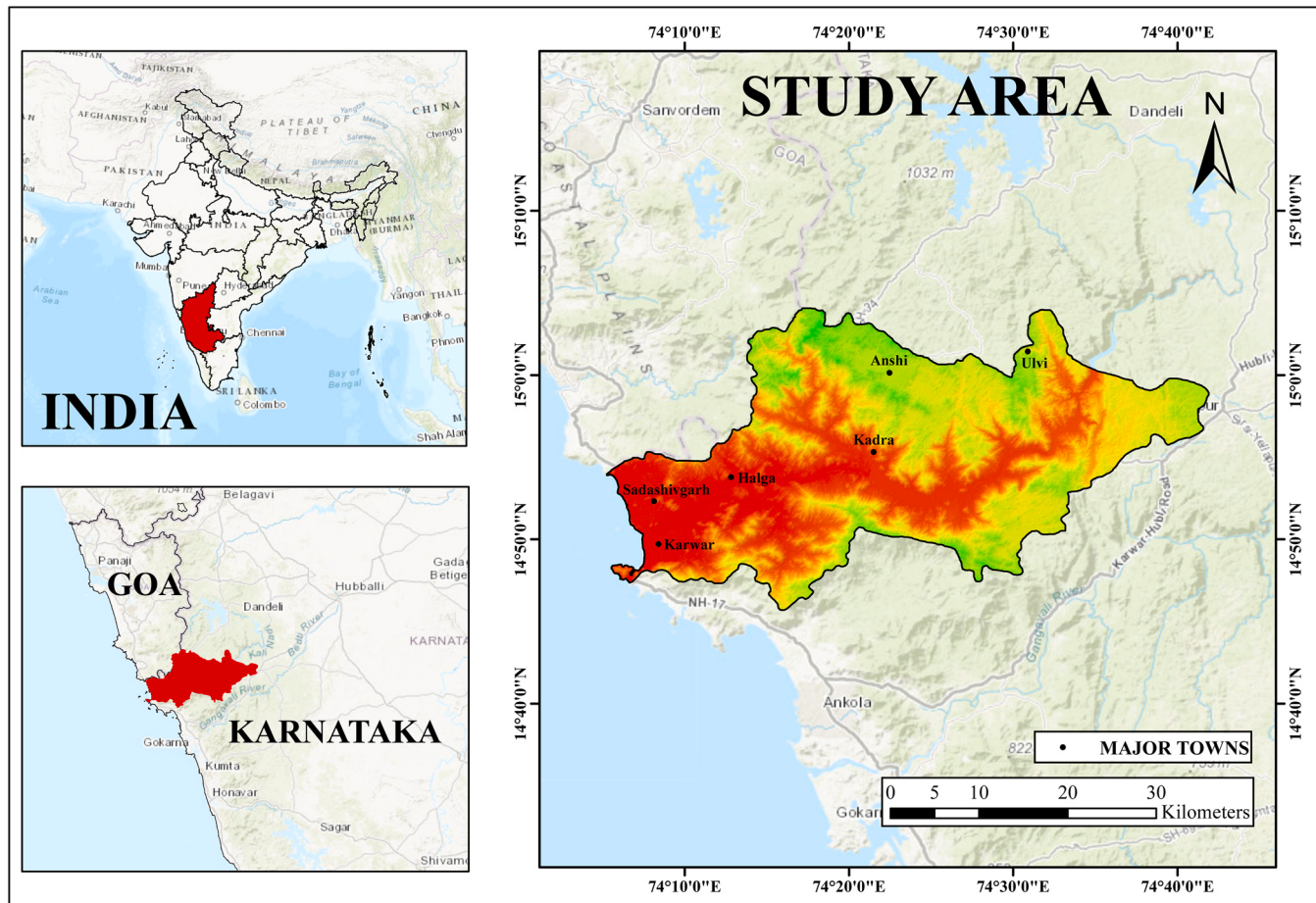


**Fig. 1.** A map showing the location of the study area.

disaster. Although the immediate disaster has passed, it has left behind significant losses and ongoing concerns about future flood events. This study aims to evaluate flood susceptibility in the region, providing critical insights that can aid authorities in mitigating the impact of similar events in the future.

#### Methodology

For the study, data was collected and processed using ArcGIS 10.8 and ENVI 5.3 software. The elevation, slope, distance from the river, rainfall, flow accumulation, stream density, soil, WRI, LULC, TWI, and SPI layers were classified using natural, equal, and manual breaks methods. AHP techniques were applied for weighting, and the flood susceptibility equation was used to generate a flood susceptibility map. The adopted methodology applied to achieving the objective of the study has been represented through the schematic diagram (Fig. 3).

#### Field investigation

A base map of the study area was prepared from toposheets of a 1:50,000 scale. A comprehensive on-site survey was conducted, based on water level indicators (Fig. 4c) and flood discharge boards (Fig. 4e and f) from Karnataka Power Corporation Limited (KPCL). Global positioning system points in flood-affected areas were gathered across the study zone. Existing flood markers were examined and distinguished. Visual documentation, encompassing images of water level indicators, water-logged cars (Fig. 4d), and collapsed structures (Fig. 4a and b) was recorded in the field. Based on the field inventories, the prepared flood susceptibility map was validated.

#### Data used

The present study utilizes the Survey of India (SOI) toposheets no: 48I/4, 48I/8, 48I/12, 48 J/1, 48 J/5, and 48 J/9 of scale 1:50,000 to prepare a base map. To supplement the analysis, Landsat 8–9 OLI (Operational Land Imager) / TIRS (Thermal Infrared) Collection 2 Level 2 data with a spatial resolution of 30 m and SRTM (Shuttle Radar Topography Mission) Digital Elevation Model (DEM) was used. Soil data was procured from the Food and Agriculture Organization (FAO) portal, scaled at 1:50,000,000. Rainfall data (2013–2022) was acquired from the Indian Meteorological Department (IMD) in a 0.25 × 0.25-degree gridded data format. All the above-discussed data was processed and analysed using the ESRI ArcGIS 10.8 and ENVI 5.3 software. Various thematic layers such as elevation, slope, distance from the river, rainfall map, flow accumulation, stream density, soil type, water ratio index (WRI), land use and land cover (LULC), topographic wetness index (TWI), and stream power index (SPI) were prepared. Utilizing the AHP model, the flood susceptibility map was generated and was further validated using the field inventories.

#### Analytical hierarchy process (AHP) model

Following the compilation of all thematic layers, the Analytical Hierarchy Process (AHP) model was employed to assign the weights to the parameters considered in this study. The AHP is a structured decision-making technique developed by Thomas L. Saaty in the 1980s. The heart of AHP involves a pairwise comparison between elements within the same hierarchy level. Decision-makers compare how important one element is to another using a relative scale (Table 1), and these



**Fig. 2.** The floodwaters have completely submerged the Kaiga township in figures a) and b). c) A vehicle parked next to a structure that has been submerged in water. d) A well that is flooded up to the parapet. e) Displays a house that has been completely submerged in water. f) Rescue operations being carried out by the naval forces despite the flooding ([Indian Navy, 2019](#), August 07).

comparisons are made for each level of the hierarchy ([Dekrita et al., 2019](#)).

The significant steps involved in the AHP model include a pairwise comparison matrix, calculation of the eigenvector ( $V_p$ ), weighting coefficient ( $C_p$ ), eigenvalue ( $\lambda_{\max}$ ), consistency index (CI), and consistency ratio (CR). Implementing the AHP in this study involves two primary segments. The major classification schemes involve categorizing all the parameters into subcategories ([Table 2](#)). The second section is constructed by categorizing all parameters based on the significance of their respective values, with assigned weights calculated for each parameter ([Table 3](#)).

For the pairwise comparison, ranks have been assigned to each parameter and subcategory based on the Saaty scale ([Table 1](#)) ([Saaty, 1980](#)) ranging from 1 to 9 (equally important to extremely important), and the other option in the pairing is assigning a rating equal to the reciprocal of this value.

The eigenvector ( $V_p$ ) and weighting coefficient ( $C_p$ ) were computed using [Eqs. \(1\)](#) and [\(2\)](#), respectively ([Danumah et al., 2016; Vilasan and Kapse, 2022](#)).

$$V_p = \sqrt[k]{W_1 \times \dots \times W_k} \quad (1)$$

where  $k$  = number of factors and  $W$ =ratings of the factors.

$$C_p = \frac{V_p}{V_p 1 + \dots + V_p k} \quad (2)$$

The sum of the weighting coefficient ( $C_p$ ) of all matrix parameters must be equal to 1.

The eigenvalue ( $\lambda_{\max}$ ) ([Eq. 3](#)), consistency index (CI) ([Eq. 4](#)) and consistency ratio (CR) ([Eq. 5](#)) can be calculated using the following equation ([Danumah et al., 2016; Bathrellos et al., 2016; Vilasan and Kapse, 2022](#)).

$$\lambda_{\max} = \frac{|E|}{k} \quad (3)$$

$$CI = \frac{(\lambda_{\max} - k)}{(k - 1)} \quad (4)$$

$$CR = \frac{CI}{RI} \quad (5)$$

Where Random Index (RI) is a critical component used to assess the consistency of the pairwise comparison matrix. The RI provides a benchmark for evaluating how consistently the comparisons have been made ([Table 4](#)).

Calculating the consistency ratio is one of the fundamental components of AHP ([Saaty, 1980](#)). The matrix is deemed adequate if the consistency ratio is less than 0.1. If the value exceeds 0.1 or 10 %, the matrix will be inconsistent, and then the ranks given must be revised ([Saaty, 1980](#)). In this study, the consistency ratio is 0.024; hence, the judgment is correct ([Table 5](#)).

The Flood Susceptibility Map (FSM) obtained through the AHP model is calculated based on the given [Eq. \(6\)](#),

$$FSM = (0.248 \times \text{Elevation}) + (0.191 \times \text{Slope}) + (0.148 \times DR) + (0.113 \times \text{Rainfall}) + (0.084 \times FA) + (0.064 \times SD) + (0.049 \times \text{Soil}) + (0.037 \times WRI) + (0.028 \times LULC) + (0.022 \times TWI) + (0.017 \times SPI) \quad (6)$$

Where DR is Distance from the River, FA is Flow Accumulation and SD is Stream Density.

#### Receiver operating characteristics (ROC) curve

To validate the flood susceptibility map, approximately 232 points

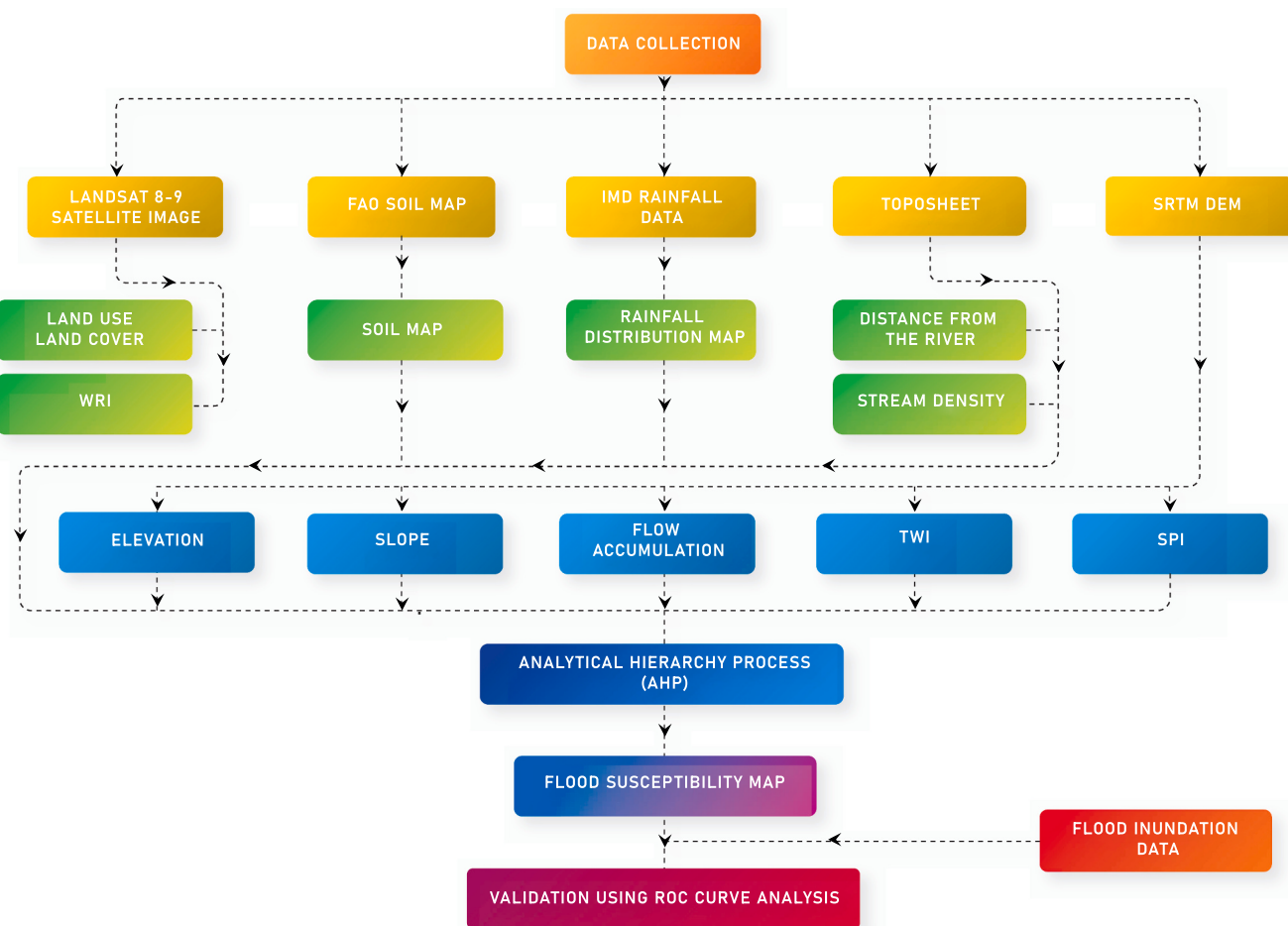


**Fig. 3.** The methodology adapted to prepare the flood susceptibility map of the study area.

were randomly sampled from the flood vulnerability dataset. The ROC curve analysis was performed using ArcSDM to assess the model's precision. The ROC curve is a well-established graphical tool for evaluating the performance of binary classification models, based on rigorous scientific principles. It offers a robust method for determining the accuracy of a model. The area under the ROC curve (AUC) is critical for evaluating the model's predictive efficacy. An AUC value of 0.5 or less indicates a model that is ineffective for flood vulnerability mapping (Vilasan and Kapse, 2022; Aichi et al., 2024). Conversely, an AUC value of 1.0 denotes a highly accurate model with excellent predictive capabilities for flood patterns (Zou et al., 2007). AUC values between 0.9 and 1.0 are considered excellent, those between 0.8 and 0.9 are deemed very good, and values from 0.7 to 0.8 are rated as good. These AUC value ranges serve as benchmarks for assessing the quality and performance of classification models.

## Results and discussion

The detailed analysis of the various causative factors for the susceptibility study and their relation to the area and spatial distribution is as follows:

### Elevation

The elevation range within the study area spans from 0 to 901 m (Fig. 5a). It has been segmented into five categories: 0–105 m, 105–252 m, 252–400 m, 400–537 m, and 537–901 m. In the context of flood mapping, elevation plays a critical role in determining the severity of flooding events (Pradhan, 2009; Bathrellos et al., 2016; Mojaddadi

et al., 2017). Elevation primarily governs the natural flow of water across the landscape, as water typically moves from higher to lower elevations due to gravitational forces. Lower-lying areas are often more susceptible to flooding as they act as gathering points for water runoff from higher elevations (Das and Pardeshi, 2018). Conversely, elevated regions often function as natural drainage basins, directing water towards lower-lying areas. Notably, this study reveals that the areas most affected by flooding are predominantly situated in lower-elevation zones.

### Slope

The gradient of the terrain serves as a regulator, influencing the movement and force of water across it. Within the study area, the slope gradient varies from 0°–15°, 15°–25°, 25°–35°, 35°–45°, and 45°–72.097° (Fig. 5b). Water can swiftly descend in regions characterized by steeper slopes, leading to accelerated runoff (Das and Pardeshi, 2018; Skilodimou et al., 2021). Steeper slopes amplify the flow velocity of water, intensifying its erosive potential and elevating the risk of downstream flash floods. The slope's inclination directly affects infiltration; the infiltration rate decreases as the slope gradient increases. This phenomenon amplifies surface runoff, leading to water accumulation in lower-lying areas and contributing to flooding, emphasizing that regions with gentler slopes (0° to 15°) are more prone to flooding.

### Distance from the river

Areas close to rivers are at a higher risk of experiencing intense flooding during heavy rainfall or when the river overflows its banks. In this study,



**Fig. 4.** The most recent flood caused the structures in figures a) and b) to collapse. c) An indication of the water level during the flooding event in 2021. d) A waterlogged vehicle during the most recent flood. e) and f) Display the flood level markings determined by the water discharge from the Kadra dam.

**Table 1**  
Saaty scale for various elements comparison (Saaty, 1980).

Scale	Judgment of Preference	Description
1	Equally important	Two factors contribute equally to the objective
3	Moderately important	Experience and judgment slightly favour one over the other
5	Important	Experience and judgment are strongly important and favour one over the other
7	Very strongly important	Experience and judgment are very strongly important and favour one over the other
9	Extremely important	The evidence favouring one over the other is of the highest possible validity
2,4,6,8	Intermediate preference between adjacent scales	When compromised is needed

the distance from the river is divided into five categories: 0–3544.03, 3544.03–7088.061, 7088.061–10632.091, 10632.091–14176.122, 14176.122–17720.152 m (Fig. 5c). The force and volume of water near rivers often intensify, resulting in more extensive structural damage and greater threats to human safety. Generally, areas near rivers are more likely to endure prolonged flooding than those farther away. This is attributed to

the slower recession of water in low-lying zones adjacent to the riverbanks. Consequently, regions situated further from the river channel exhibit lower vulnerability to flood occurrences (Das, 2018). Therefore, the areas within the 0–3544.03 m range from the river are significantly predisposed to flooding.

#### Rainfall

Rainfall intensity significantly contributes to flood development. Rainfall within the study area has been classified into five categories: 1902.95–2321.826, 2321.826–2721.651, 2721.651–3109.125, 3109.125–3479.408, and 3479.408–3817.227 millimetres per year (Fig. 5d). The annual rainfall trend from 2013 to 2022 is depicted in Fig. 6. When the rainfall rate surpasses the soil's capacity for infiltration, excess water accumulates in low-lying areas, streams, and rivers. Intense and rapid rainfall within a condensed timeframe can lead to rivers overflowing and subsequent flooding. The study region is characterized by a tropical monsoon climate, with the majority of its annual rainfall, ranging from 75 % to 90 %, occurring between June and September due to the southwest orographic monsoon. Notably, the years 2019, 2020 and 2021 witnessed the highest annual rainfall levels in the study area.

**Table 2**

Sub-criteria of each parameter along with pairwise comparison matrix and their weights.

SL. NO.	Factors	1	2	3	4	5	CR	CP
1	<b>Elevation</b>						0.007	
	<105	1	2	4	6	9	0.475	
	105 – 252	1/	1	2	4	6	0.267	
	2							
	252 – 400	1/	1/	1	2	4	0.141	
	4	2						
	400 – 537	1/	1/	1/	1	2	0.075	
	6	4	2					
	537<	1/	1/	1/	1/	1	0.042	
	9	6	4	2				
2	<b>Slope</b>						0.007	
	<15	1	2	4	6	9	0.475	
	15 – 25	1/	1	2	4	6	0.267	
	2							
	25 – 35	1/	1/	1	2	4	0.141	
	4	2						
	35 – 45	1/	1/	1/	1	2	0.075	
	6	4	2					
	45<	1/	1/	1/	1/	1	0.042	
	9	6	4	2				
3	<b>Distance from the River (DR)</b>						0.010	
	<3544.03	1	2	4	6	8	0.469	
	3544.03 – 7088.061	1/	1	2	4	6	0.269	
	2							
	7088.061 – 10632.091	1/	1/	1	2	4	0.143	
	4	2						
	10632.091 – 14176.122	1/	1/	1/	1	2	0.076	
	6	4	2					
	14176.122<	1/	1/	1/	1/	1	0.043	
	8	6	4	2				
4	<b>Rainfall</b>						0.054	
	<2321.826	1	1/	1/	1/	1/	0.033	
	3	5	7	9				
	2321.826 – 2721.651	3	1	1/	1/	1/	0.064	
	2721.651 – 3109.125	3	5	7				
	3109.125 – 3479.408	5	3	1	1/	1/	0.130	
	3479.408 – 3479.408<	7	5	3	1	1/	0.264	
	9	7	5	3	1			
5	<b>Flow Accumulation (FA)</b>						0.004	0.510
	<20656	1	1/	1/	1/	1/	0.050	
	2	3	5	8				
	20656 – 84165	2	1	1/	1/	1/	0.088	
	3		2	3	5			
	84165 – 210949	3	2	1	1/	1/	0.151	
	2		3	2	3			
	210949 – 453112	5	3	2	1	1/	0.259	
	2		3	2	1			
6	<b>Stream Density (SD)</b>						0.054	0.452
	<1.836	1	3	5	7	9	0.510	
	1.836 – 3.586	1/	1	3	5	7	0.264	
	3							
	3.586 – 5.08	1/	1/	1	3	5	0.130	
	5	3						
	5.08 – 6.745	1/	1/	1/	1	3	0.064	
	7	5	3					
	6.745<	1/	1/	1/	1/	1	0.033	
	9	7	5	3				
7	<b>Soil</b>						0.054	
	Sandy	1	1/	1/	1/	1/	0.033	
	3	5	7	9				
	Sandy Loamy	3	1	1/	1/	1/	0.064	
	3		5	7				
	Clayey-Skeletal	5	3	1	1/	1/	0.130	
	3		5	7				
	Clay Loamy	7	5	3	1	1/	0.264	
	3		5	7				
	Clayey	9	7	5	3	1	0.510	

**Table 2 (continued)**

SL. NO.	Factors	1	2	3	4	5	CR	CP
8	<b>WRI</b> <0.597	1	1/	1/	1/	1/	0.054	0.033
		3	5	7	9			
	0.597 – 0.643	3	1	1/	1/	1/	0.064	
		3	5	7				
	0.643 – 0.745	5	3	1	1/	1/	0.130	
		3	5					
	0.745 – 0.942	7	5	3	1	1/	0.264	
		3	5	7				
	0.942<	9	7	5	3	1	0.510	
9	<b>LULC</b> Forest	1	1/	1/	1/	1/	0.026	0.050
		3	5	9				
	Barren Land	3	1	1/	1/	1/	0.114	
		3	5					
	Built-Up	5	3	1	1/	1/	0.255	
		3	5	7				
	Waterbody	9	5	3	1		0.581	
10	<b>TWI</b> <5.925	1	1/	1/	1/	1/	0.054	0.033
		3	5	7	9			
	5.925 – 7.956	3	1	1/	1/	1/	0.064	
		3	5	7				
	7.956 – 11.002	5	3	1	1/	1/	0.130	
		3	5					
	11.002 – 14.895	7	5	3	1	1/	0.264	
		3	5	7				
	14.895<	9	7	5	3	1	0.510	
11	<b>SPI</b> ≤-6.371	1	3	5	7	9	0.510	
		1/	1	3	5	7	0.264	
	-6.371 – -2.387	3						
	-2.387 – -0.08	1/	1/	1	3	5	0.130	
	-0.08 – 2.541	1/	1/	1/	1	3	0.064	
		7	5	3				
	2.541<	1/	1/	1/	1/	1	0.033	
	9	7	5	3				

#### Flow accumulation

In hydrological studies, flow accumulation is a fundamental component in watershed modelling and flood prediction. The gradient of flow accumulation in the study region has been classified into five distinct classes: 0–20656, 20656–84165, 84165–210949, 210949–453112, and 453112–981707 (Fig. 5e). Flow accumulation is based on the principle that water flows downhill and accumulates through a river network. Locations characterized by high flow accumulation are likely to exhibit increased vulnerability to flooding (Tehrany et al., 2015). In the upper reaches of the study area, flow accumulation tends to be relatively low due to the prevalence of lower-order streams. As one progresses downstream, flow accumulation steadily increases as tributaries converge with the primary channel, amplifying flood susceptibility. Notably, the downstream region (453112–981707) of the study area exhibits the highest levels of flow accumulation, consequently heightening the risk of flooding.

#### Stream density

Stream density, a term within geomorphology, denotes the extent of stream channel length within a specific geographic area. In the context of this study, stream density was categorized into five distinct classes: 0–1.836, 1.836–3.586, 3.586–5.08, 5.08–6.745, and 6.745–10.929 kilometre per square kilometre (Fig. 5f). Typically, it is calculated by dividing the collective length of all stream channels within a given region by the total area of that same region (Vilasan and Kapse, 2022). Elevated stream density values signify a dense network of streams and rivers, implying a well-developed drainage system and heightened

**Table 3**

Pairwise comparison matrix and relative score of each parameter.

Pairwise matrix	Elevation	Slope	DR	Rainfall	FA	SD	Soil	WRI	LULC	TWI	SPI	Vp	Cp
Elevation	1	2	2	3	4	4	5	6	7	8	9	3.868	0.248
Slope	1/2	1	2	2	3	4	4	5	6	7	8	2.975	0.191
DR	1/2	1/2	1	2	2	3	4	4	5	6	7	2.312	0.148
Rainfall	1/3	1/2	1/2	1	2	2	3	4	4	5	6	1.753	0.113
FA	1/4	1/3	1/2	1/2	1	2	2	3	4	4	5	1.313	0.084
SD	1/4	1/4	1/3	1/2	1/2	1	2	2	3	4	4	1	0.064
Soil	1/5	1/4	1/4	1/3	1/2	1/2	1	2	2	3	4	0.762	0.049
WRI	1/6	1/5	1/4	1/4	1/3	1/2	1/2	1	2	2	3	0.57	0.037
LULC	1/7	1/6	1/5	1/4	1/4	1/3	1/2	1/2	1	2	2	0.433	0.028
TWI	1/8	1/7	1/6	1/5	1/4	1/4	1/3	1/2	1/2	1	2	0.336	0.022
SPI	1/9	1/8	1/7	1/6	1/5	1/4	1/4	1/3	1/2	1/2	1	0.259	0.017
Sum	3.579	5.468	7.343	10.2	14.033	17.833	22.583	28.333	35	42.5	51	15.58	1

**Table 4**

Random index matrix of the same dimension (Saaty, 1980).

Number of Criteria	2	3	4	5	6	7	8	9	10	11
RI	0.00	0.58	0.90	1.12	1.24	1.32	1.41	1.45	1.49	1.51

potential for efficient water flow. Conversely, lower stream density values indicate a sparser network of streams, suggesting less efficient drainage and slower water movement, consequently increasing the risk of flooding. Importantly, regions characterized by low stream density (0–1.836) exhibit higher susceptibility to flooding.

#### Soil

Soil plays a crucial role in influencing flood behaviour and can either exacerbate or mitigate the impact of flooding events. Within the study area, five distinct soil types are present: sandy ( $7.94 \text{ km}^2$ ), sandy loamy ( $131.32 \text{ km}^2$ ), clayey skeletal ( $767.78 \text{ km}^2$ ), clay loamy ( $15.18 \text{ km}^2$ ), and clayey ( $253.23 \text{ km}^2$ ) (Fig. 7a). The infiltration capacity of the soil significantly affects flood potential. Soils with high infiltration rates can promptly absorb rainfall, facilitating water penetration into the ground and reducing surface runoff. Additionally, soils with low infiltration rates contribute to heightened runoff and increased flood susceptibility (Gregory et al., 2006). The steady-state infiltration rates for different soil types vary: sand has an infiltration rate  $> 0.8 \text{ in/h}$ , loam ranges from 0.2 to 0.4 in/h, and clay falls between 0.04 and 0.2 in/h (Vilasan and Kapse, 2022). The findings of this study indicate that areas characterized by clayey and sandy loamy soil types were more vulnerable to flooding than the rest.

#### WRI

The water ratio index of the study area was categorized into five distinct classes ranging from 0.462 to 0.597, 0.597–0.643, 0.643–0.745, 0.745–0.942, and 0.942–1.304 (Fig. 7b). WRI values above 1 are considered the presence of water (Shen and Li, 2010). An area characterized by higher WRI values exhibits increased chances of flooding. Extracting water body information from remotely sensed images is important for surveying, planning, and safeguarding water resources, especially for managing flood disasters through monitoring, evaluation, emergency response, and other means.

#### LULC

Land cover classification in a region is typically established based on the presence and characteristics of vegetation, which in turn sheds light on its usage, environmental conditions, agricultural practices, and seasonal variations in plant life (El Morjani et al., 2017). The LULC of the study area was divided into four categories: Forest 80 % ( $940 \text{ km}^2$ ), Built-up 1.5 % ( $17.63 \text{ km}^2$ ), Barren land 13 % ( $152.75 \text{ km}^2$ ), and

Waterbody 5.5 % ( $64.63 \text{ km}^2$ ) (Fig. 7c). Urbanization and the conversion of natural landscapes into impermeable surfaces, such as pavement, concrete, and buildings, diminish the land's capacity to absorb rainfall. Instead of permeating the soil, rainwater rapidly runs off these surfaces, intensifying the volume and speed of surface runoff. This phenomenon can lead to swift and intense flooding, commonly called flash floods (Gigović et al., 2017), as water accumulates in low-lying regions or overwhelms drainage systems. Strategic land use planning and floodplain management are pivotal in mitigating flood risks. The impact of flooding can be diminished by avoiding development in flood-prone areas, maintaining natural water retention zones, and implementing appropriate stormwater management strategies. Notably, built-up and barren land areas situated close to water bodies exhibit a higher vulnerability to flooding in the study area.

#### TWI

The Topographic Wetness Index (TWI) is a terrain-based parameter that quantifies the potential wetness or water saturation of an area based on its topography (Mojaddadi et al., 2017; Das, 2018). TWI is closely linked to soil moisture content and characteristics, significantly impacting infiltration capacity. The TWI within this specific river basin spans from 2.456 to 24.118. In the context of the current study, the TWI has been divided into five distinct classes (Fig. 7d): 2.456–5.925, 5.925–7.956, 7.956–11.002, 11.002–14.895, and 14.895–24.118. This classification underscores the correlation between higher TWI gradients and increased vulnerability to flooding. Notably, regions characterized by a TWI gradient of 14.895–24.118 are more likely to experience more frequent flood occurrences, thus emphasizing the role of topography in influencing flood susceptibility.

#### SPI

The Stream Power Index (SPI) is a parameter used to quantify the erosive strength of a stream or river, which is determined by its slope and discharge (Altin and Gökkaya, 2015). In this study, SPI has been categorized into five classes: -13.816 to -6.371, -6.371 to -2.387, -2.387 to -0.08, -0.08 to 2.541, and 2.541–13.027 (Fig. 7e). Higher SPI values correspond to steeper slopes and more significant stream discharges, indicating increased potential for channel erosion and contributing to channel widening and deepening. Additionally, stream force is diminished in regions characterized by low SPI values, resulting in shallow channels and meandering. This can lead to sediment accumulation along the banks (Vilasan and Kapse, 2022), which has been

**Table 5**  
Normalization matrix.

Normalized matrix	Elevation	Slope	DR	Rainfall	FA	SD	Soil	WRI	LULC	TWI	SPI	SUM	C	D	E	$\lambda_{\max}$	CI	CR
Elevation	0.28	0.37	0.27	0.29	0.22	0.21	0.2	0.19	0.18	0.27	0.25	2.86	11.57	11.37	0.037	0.024		
Slope	0.14	0.18	0.27	0.2	0.21	0.22	0.18	0.17	0.16	0.16	0.19	2.2	11.64					
DR	0.14	0.09	0.14	0.2	0.14	0.17	0.18	0.14	0.14	0.14	0.14	1.61	0.15	1.7	11.59			
Rainfall	0.09	0.09	0.07	0.1	0.14	0.11	0.13	0.14	0.11	0.12	0.12	1.23	0.11	1.29	11.55			
FA	0.07	0.06	0.07	0.05	0.07	0.11	0.09	0.11	0.11	0.09	0.1	0.93	0.08	0.97	11.45			
SD	0.07	0.05	0.05	0.05	0.04	0.06	0.09	0.07	0.09	0.09	0.08	0.72	0.07	0.74	11.31			
Soil	0.06	0.05	0.03	0.03	0.04	0.03	0.04	0.07	0.06	0.07	0.08	0.55	0.05	0.56	11.19			
WRI	0.05	0.04	0.03	0.02	0.02	0.03	0.02	0.04	0.06	0.05	0.06	0.41	0.04	0.42	11.15			
LULC	0.04	0.03	0.03	0.03	0.02	0.02	0.02	0.02	0.03	0.05	0.04	0.31	0.03	0.32	11.16			
TWI	0.03	0.03	0.02	0.02	0.02	0.02	0.01	0.01	0.01	0.02	0.02	0.24	0.02	0.25	11.16			
SPI	0.03	0.02	0.02	0.02	0.01	0.01	0.01	0.01	0.01	0.01	0.02	0.19	0.02	0.19	11.29			
<b>SUM</b>	<b>1</b>	<b>1</b>	<b>1</b>	<b>1</b>	<b>1</b>	<b>1</b>	<b>1</b>	<b>1</b>	<b>1</b>	<b>1</b>	<b>1</b>	<b>11</b>	<b>1</b>	<b>125.06</b>				

recognized as a significant contributor to flooding in areas near the base level of the river. It has been observed that regions characterized by a low SPI gradient (-13.816 to -6.371) exhibit a higher vulnerability to flooding.

#### Flood susceptibility mapping

The flood susceptibility mapping (FSM) is the most critical step in the present study to understand and analyse the flood risk and hazard of the study area. A flood susceptibility map indicates the likelihood or probability of specific areas being impacted by floods. It is a visual representation that highlights regions more susceptible to flooding, drawing upon a spectrum of factors encompassing terrain, land usage, rainfall patterns, hydrological attributes, and historical flood records. The eleven selected conditioning factors were subjected to resampling (30 m × 30 m), reclassification (utilizing natural breaks, manual assessment, and equal divisions), and subsequently employed in calculating the FSM (30 m × 30 m) through Eq. (6). The resultant flood susceptibility map was categorized (using natural break) into five categories: very-high, high, moderate, low, and very-low (Fig. 8) (Karpouza et al., 2023). These categories collectively comprise 14.87 %, 16.07 %, 18.26 %, 28.54 %, and 22.27 % of the total study area, as indicated in Table 6.

The central and western coastal regions of the study area notably encompass the very high and highly susceptible zones. Slopes surpassing 15° in these areas discourage water pooling and stagnation, while abundant dense vegetation and level terrain facilitate surface water retention during flooding (Zaharia et al., 2017). Notably, the highly susceptible zones exhibit lower elevation, slope, and SPI values, contributing to enhanced water accumulation. This phenomenon is linked to the reduced river velocity resulting from lower elevation and slope, leading to sediment deposition in overbank areas and consequent flooding (Sarkar and Mondal, 2020). In contrast, regions characterized by higher slopes exhibit lower susceptibility to flooding (Das, 2018).

Furthermore, the eastern and northern portions of the study area exhibit a low to very low likelihood of flooding, attributed to elevated elevations and slopes exceeding 40°. These areas experience rapid stream flow from the Western Ghats escarpments, minimizing water retention and thus displaying the minimal probability of flooding. Stream density plays a counteractive role in flood susceptibility. Typically, areas with high elevation and slopes exhibit a steeper stream density gradient. Natural water flow velocity is optimised in regions with higher stream density, consequently minimizing water accumulation. Validation of the prepared flood susceptibility map is paramount to confirm its reliability. The ROC model was applied for this purpose, furnishing insight into the accuracy of the flood susceptibility map by evaluating its results against the actual scenario.

#### Validation of the flood susceptibility map

The prepared flood susceptibility map has exhibited significant efficacy and accuracy in identifying vulnerable regions through the application of the AHP method. To validate this map, flood points collected from field investigations were integrated with flood vulnerability index (FVI) data sourced from the National Remote Sensing Centre (NRSC) database. In this study, the ROC curve analysis yielded an AUC value of 0.829 (Fig. 9). This AUC value indicates that the model possesses strong discriminatory power, effectively distinguishing between flood-prone and non-flood-prone areas. The high AUC value underscores the model's reliability and efficacy, confirming the acceptability of the results for further modelling endeavours. These findings reinforce the model's applicability and reliability in real-world scenarios, making it a valuable tool for future flood susceptibility and risk mitigation efforts.

#### Adaptive measures

The study area has experienced recurrent flooding (KSDMA, 2019),

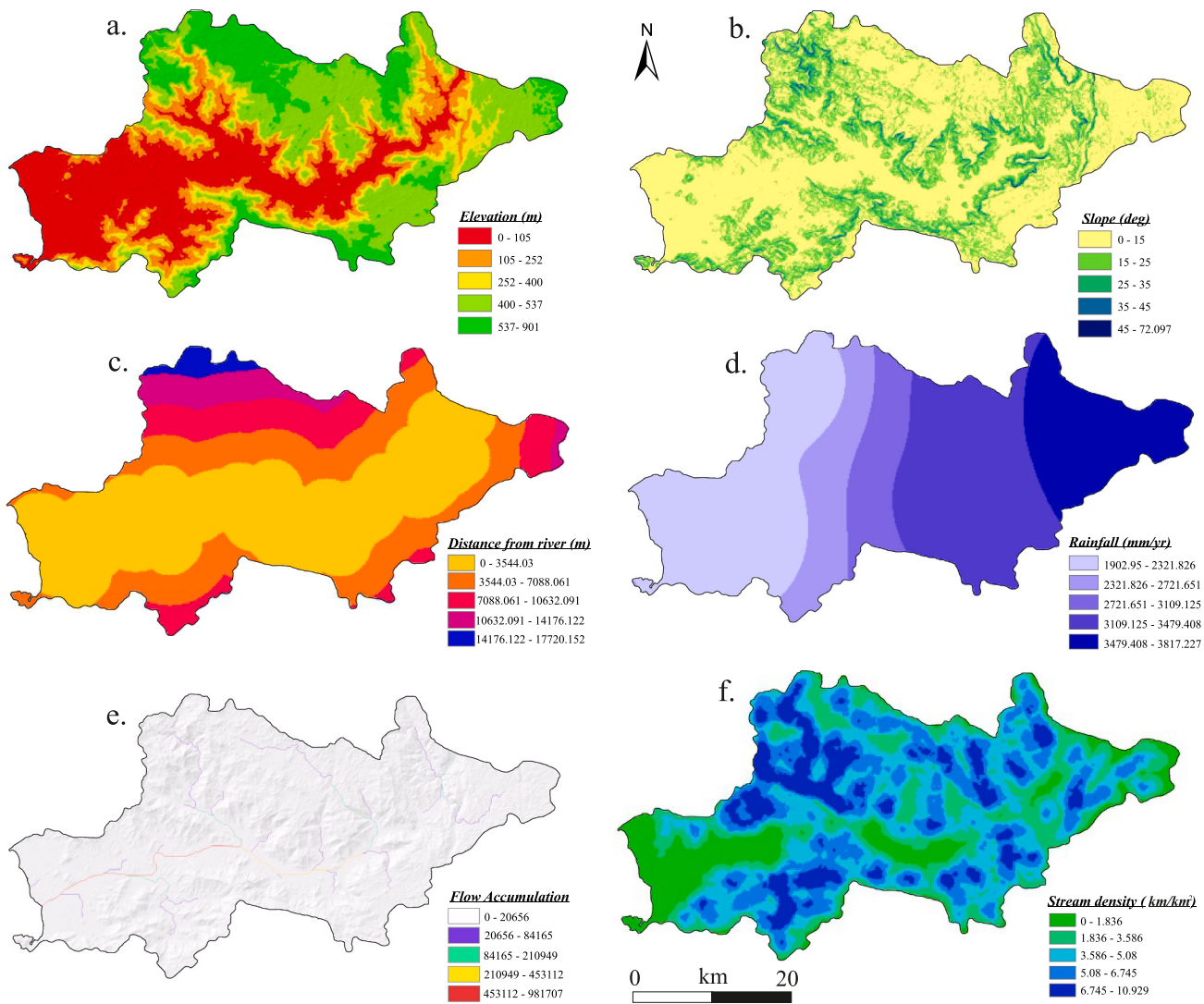


**Fig. 5.** a) Altitudinal variation, b) Slope gradient, c) Distance from the river d) Rainfall distribution, e) Flow accumulation, f) Stream density.

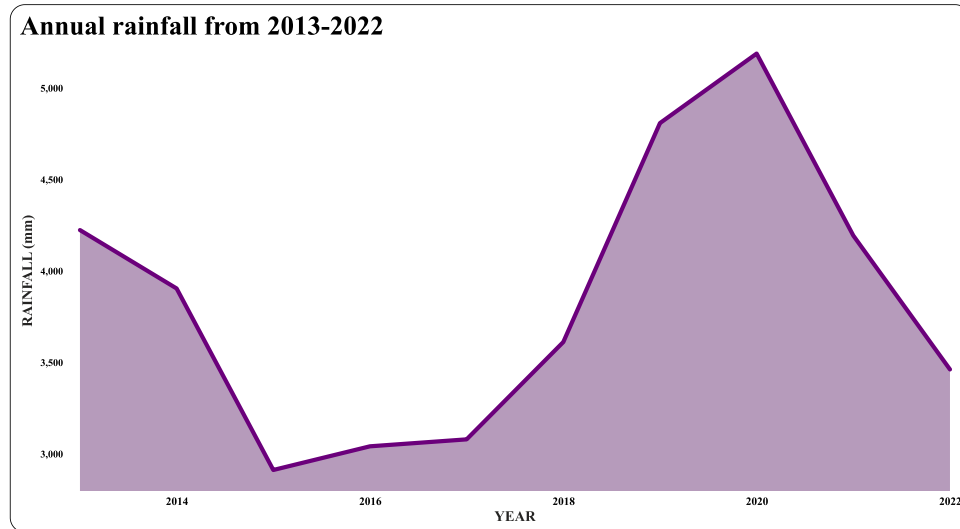


**Fig. 6.** Trend of annual rainfall from 2013 to 2022.

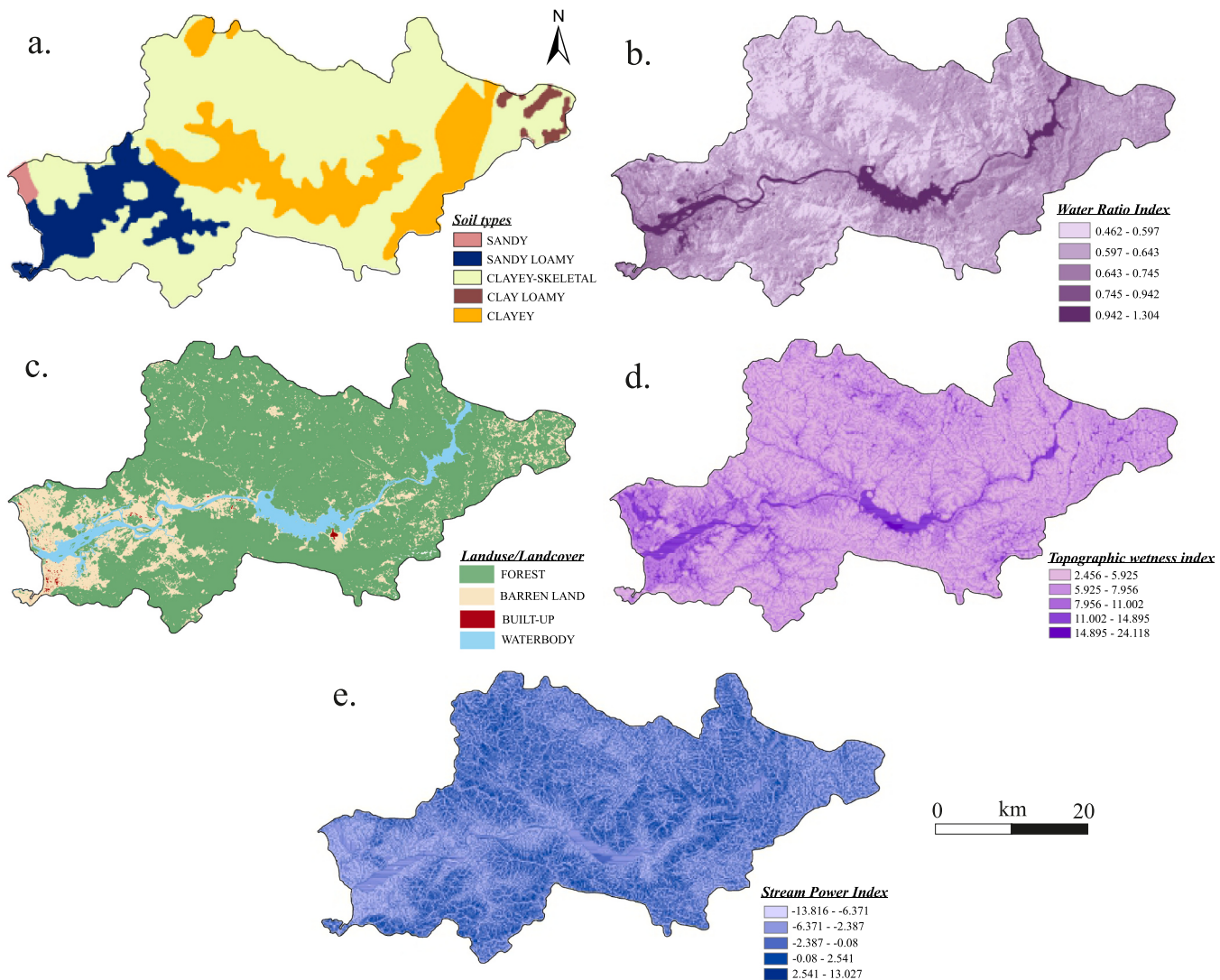


**Fig. 7.** a) Soil type, b) Water ratio index (WRI), c) Land use pattern, d) Topographic wetness index (TWI), e) Stream power index (SPI).

emphasising the need to depict them as high-risk zones susceptible to natural forces and human influences. Crafting a practical management approach entails integrating comprehensive data, advanced techniques, specialised equipment, and thorough analysis to mitigate the adverse effects of these floods. The interplay of natural elements like orographic rainfall and human-driven actions such as construction in vulnerable regions contribute to the flooding in this study area. However, implementing a well-structured management strategy is critical to substantially curtailing the impact of these floods. The primary step to be considered to reduce the intensity of the flood in the study area is,

- To create and maintain natural buffer zones, such as wetlands and floodplain forests, which can absorb excess water and mitigate flood impacts. These areas also provide recreational spaces during non-flood times.
- Implement strict zoning regulations that restrict construction in high-risk flood areas. Encourage the relocation of vulnerable infrastructure and buildings to safer locations.
- Establish a robust early warning system integrating real-time weather monitoring, dam water level sensors, and predictive models. This system will provide timely alerts to residents, local authorities, and emergency responders, allowing them to take necessary actions in advance.

- Create a proper design and mark evacuation routes that lead to higher ground or safe shelters. Ensure these routes are well-maintained and accessible to all, including those with disabilities.
- Identify and designate safe shelters on higher ground that can accommodate a significant number of people. Stock these shelters with emergency supplies, such as food, water, medical kits and blankets.

## Conclusions

This study attempted to construct a comprehensive flood susceptibility map for the base-level subbasin of the Kali River, situated at the foothills of the Western Ghats. The flood susceptibility map was categorized into five classes: very high, high, moderate, low, and very low. Within the study zone,  $360.59 \text{ km}^2$  (30 %) were identified as high susceptibility areas. These regions are predominantly situated in the west-central portion of the study area, proximate to the Kali River. The ROC curve analysis result of 0.829 indicates the stability of the FSM model prepared using AHP. The flood event in this locale was attributed to a combination of natural and human-induced factors. The findings from this investigation hold potential value for decision-makers, planners, and governing bodies, offering insights that can contribute to the sustainable management and mitigation of floods within the studied region. The method used in this research underscores its significance in

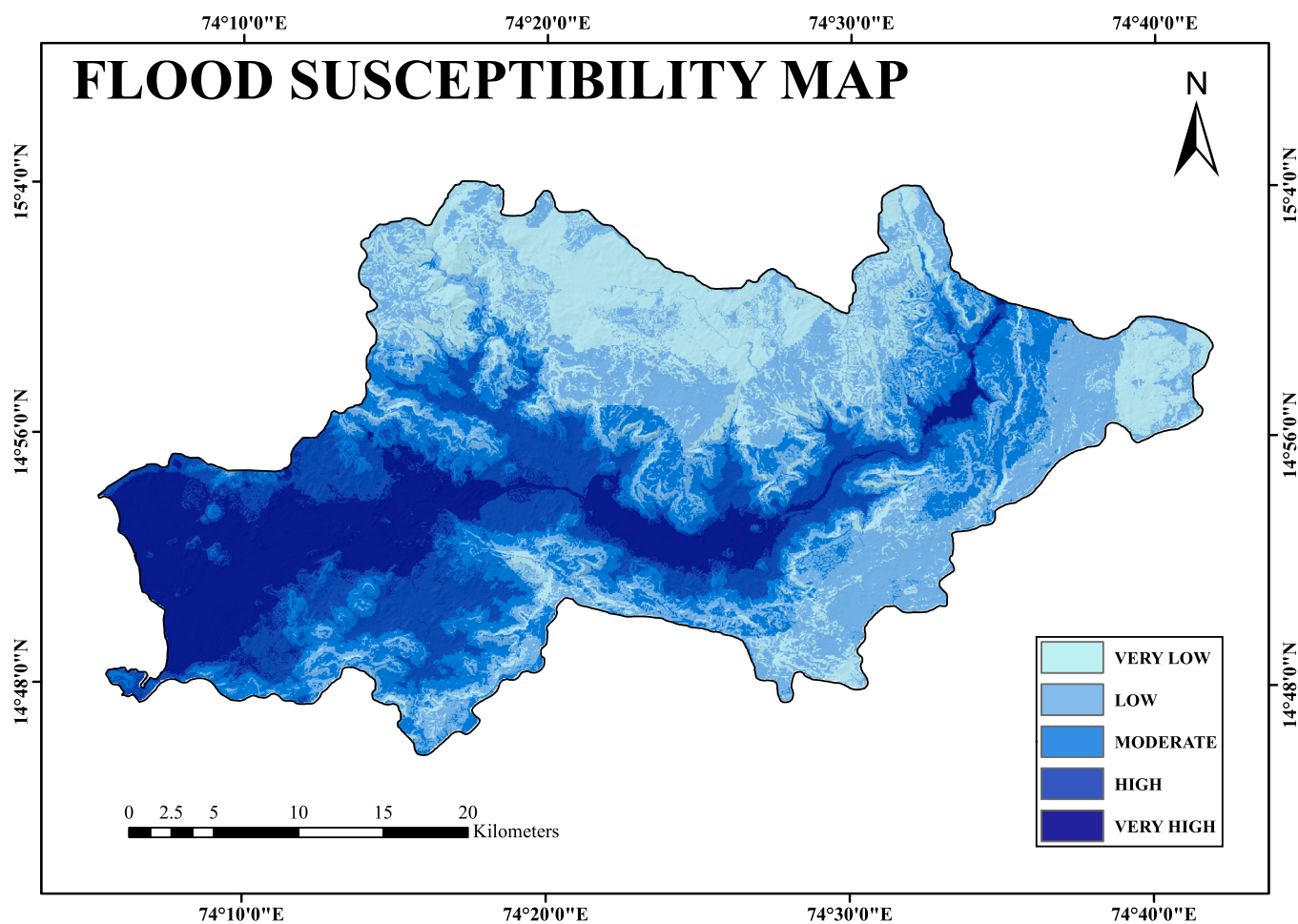


**Fig. 8.** Flood susceptibility map.

**Table 6**  
Area and percentage of flood susceptible zones.

Susceptible zones	AHP METHOD	
	Area of susceptible zones (sq. km)	Percentage of susceptible zones
Very low	259.54	22.27
Low	332.67	28.54
Moderate	212.80	18.26
High	187.28	16.07
Very high	173.31	14.87

evaluating flood vulnerabilities across various geographical settings globally. This adaptability is attributed to its capacity to produce reasonably precise outcomes. However, while recognizing the generalized classification of several influencing factors such as elevation, slope, proximity to the river, and rainfall, it is recommended to meticulously assess flood susceptibility for specific catchment areas within the study region. Such a tailored evaluation can yield more intricate and precise estimations of flood likelihood at a local scale.

#### CRediT authorship contribution statement

**Krishnan Ananda:** Writing – original draft, Visualization, Software, Methodology, Investigation, Formal analysis, Data curation, Conceptualization. **S. G Dhanil Dev:** Writing – original draft, Visualization, Validation, Supervision, Methodology, Investigation, Formal analysis, Conceptualization. **Arjun S.:** Writing – original draft, Visualization, Software, Formal analysis, Data curation. **Deepchand V.:** Writing –

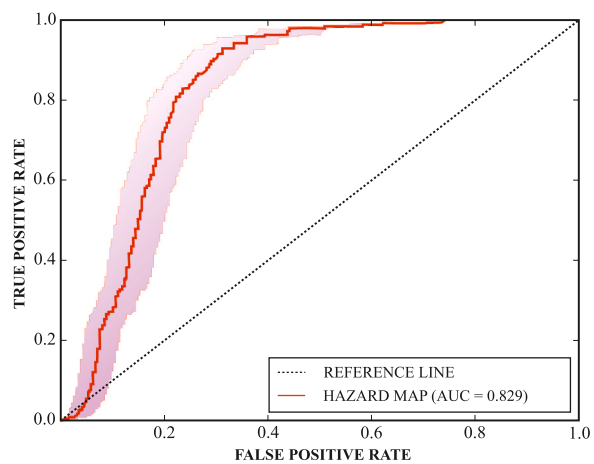


**Fig. 9.** The ROC Curve.

original draft, Software, Methodology, Investigation, Formal analysis, Data curation, Conceptualization. **Singh Yogendra:** Writing – review & editing, Validation, Supervision, Investigation, Formal analysis. **Shaji E.:** Validation, Supervision, Formal analysis, Conceptualization. **Krishnaprasad P.K.:** Visualization, Software.

#### Declaration of Competing Interest

The authors declare that they have no known competing financial

interests or personal relationships that could have appeared to influence the work reported in this paper.

## Acknowledgement

The authors extend their heartfelt gratitude to the villagers and officials from Kaiga township for their generosity in sharing the invaluable photographs documenting the devastating flood of 2019 that impacted the region. Their cooperation and willingness to provide these visual insights have significantly enriched this research. Special appreciation is also extended to Megha R., Research Scholar, Department of Geology, whose invaluable assistance during the fieldwork.

## Data availability

No data was used for the research described in the article.

## References

- Acreman, M., Holden, J., 2013. How wetlands affect floods. *Wetlands* 33, 773–786.
- Aichi, A., Ikirri, M., Haddou, M.A., Quesada-Román, A., Sahoo, S., Singha, C., Abiou, M., 2024. Integrated GIS and analytic hierarchy process for flood risk assessment in the Dades Wadi watershed (Central High Atlas, Morocco). *Results Earth Sci.* 2, 100019.
- Ali, S.A., Parvin, F., Pham, Q.B., Vojtek, M., Vojteková, J., Costache, R., Ghorbani, M.A., 2020. GIS-based comparative assessment of flood susceptibility mapping using hybrid multi-criteria decision-making approach, naïve Bayes tree, bivariate statistics and logistic regression: a case of Topľa basin, Slovakia. *Ecol. Indic.* 117, 106620.
- Allaire, M., 2018. Socio-economic impacts of flooding: A review of the empirical literature. *Water Secur.* 3, 18–26 (s).
- Altin, T.B., Gökkaya, E., 2015. Landslide-Triggering Factors in Korucak Subbasin, North Anatolian, Turkey. *Procedia Earth Planet. Sci.* 15, 566–572.
- Bathrellos, G.D., Karymbalis, E., Skilodimou, H.D., Gaki-Papanastassiou, K., Baltas, E.A., 2016. Urban flood hazard assessment in the basin of Athens Metropolitan city, Greece. *Environ. Earth Sci.* 75, 1–14.
- Bronstert, A., 2003. Floods and climate change: interactions and impacts. *Risk Anal.: Int. J.* 23 (3), 545–557.
- Charlton, R., Fealy, R., Moore, S., Sweeney, J., Murphy, C., 2006. Assessing the impact of climate change on water supply and flood hazard in Ireland using statistical downscaling and hydrological modeling techniques. *Clim. Change* 74 (4), 475–491.
- Christensen, J.H., Christensen, O.B., 2003. Severe summertime flooding in Europe. *Nature* 421 (6925), 805–806.
- Danumah, J.H., Odai, S.N., Saley, B.M., Szarzynski, J., Thiel, M., Kwaku, A., Akpa, L.Y., 2016. Flood risk assessment and mapping in Abidjan district using multi-criteria analysis (AHP) model and geoinformation techniques, (côte d'ivoire). *Geoenviron. Disasters* 3, 1–13.
- Das, S., 2018. Geographic information system and AHP-based flood hazard zonation of Vaitarna basin, Maharashtra, India. *Arab. J. Geosci.* 11 (19), 576.
- Das, S., Pardeshi, S.D., 2018. Morphometric analysis of Vaitarna and Ulhas River basins, Maharashtra, India: using geospatial techniques. *Appl. Water Sci.* 8, 1–11.
- Das, S., Gupta, A., Ghosh, S., 2017. Exploring groundwater potential zones using MIF technique in a semi-arid region: a case study of Hingoli district, Maharashtra. *Spat. Inf. Res.* 25, 749–756.
- Dekrita, Y.A., Yunus, R., Citta, A.B., Yamin, M., 2019. Integration of balanced scorecard and analytical hierarchy process as a tool for determining the priority of the program strategy: case study in Dr. Tc. Hillers Maumere hospital (August). In 3rd International Conference on Accounting, Management and Economics 2018 (ICAME 2018). Atlantis Press, pp. 71–84 (August).
- Dou, X., Song, J., Wang, L., Tang, B., Xu, S., Kong, F., Jiang, X., 2018. Flood risk assessment and mapping based on a modified multi-parameter flood hazard index model in the Guanzhong Urban Area, China. *Stoch. Environ. Res. Risk Assess.* 32, 1131–1146.
- El Morjani, Z.E.A., Seif Ennasr, M., Elmouden, A., Idibraim, S., Bouaakaz, B., Saad, A., 2017. Flood hazard mapping and modeling using GIS applied to the Souss river watershed. *Souss-Mass. River Basin, Moroc.* 57–93.
- Gigović, L., Pamucar, D., Bajić, Z., Drobnjak, S., 2017. Application of GIS-interval rough AHP methodology for flood hazard mapping in urban areas. *Water* 9 (6), 360.
- Gregory, J.H., Dukes, M.D., Jones, P.H., Miller, G.L., 2006. Effect of urban soil compaction on infiltration rate. *J. Soil Water Conserv.* 61 (3), 117–124.
- Guo, E., Zhang, J., Ren, X., Zhang, Q., Sun, Z., 2014. Integrated risk assessment of flood disaster based on improved set pair analysis and the variable fuzzy set theory in central Liaoning Province, China. *Nat. Hazards* 74, 947–965.
- Hong, H., Panahi, M., Shirzadi, A., Ma, T., Liu, J., Zhu, A.X., Kazakis, N., 2018. Flood susceptibility assessment in Hengfeng area coupling adaptive neuro-fuzzy inference system with genetic algorithm and differential evolution. *Sci. Total Environ.* 621, 1124–1141.
- Indian Navy. (2019, August 07). Naval base Karwar provides assistance to civil administration – Update 1. Retrieved from (<https://www.indiannavy.nic.in/content/naval-base-karwar-provides-assistance-civil-administration-%E2%80%99update-1>).
- Karpouza, M., Bathrellos, G.D., Kaviris, G., Antonarakou, A., Skilodimou, H.D., 2023. How could students be safe during flood and tsunami events? *Int. J. Disaster risk Reduct.* 95, 103830.
- Kazakis, N., Koulias, I., Patsialis, T., 2015. Assessment of flood hazard areas at a regional scale using an index-based approach and Analytical Hierarchy Process: Application in Rhodope-Evros region, Greece. *Sci. Total Environ.* 538, 555–563.
- Krishnan, A., 2024. Morphometric analysis in the sub basins of the Kali River using Geographic Information System, Karnataka, India. *Geomatica* 76 (2), 100013.
- KSDMA). (2019). Karnataka State Disaster Management Plan 2019-20. Bengaluru, India: BBMP Government Website. (<https://webapps.bbmpgov.in/dm-apply/Images/final-english-ksdmp-2019-20.pdf>).
- Merkuryeva, G., Merkuryev, Y., Sokolov, B.V., Potryasaev, S., Zelentsov, V.A., Lektauers, A., 2015. Advanced river flood monitoring, modelling and forecasting. *J. Comput. Sci.* 10, 77–85.
- Mojaddadi, H., Pradhan, B., Nampak, H., Ahmad, N., Ghazali, A.H.B., 2017. Ensemble machine-learning-based geospatial approach for flood risk assessment using multi-sensor remote-sensing data and GIS. *Geomat., Nat. Hazards, Risk* 8 (2), 1080–1102.
- Nourani, V., Tahershamsi, A., Abbaszadeh, P., Shahrabi, J., Hadavandi, E., 2014. A new hybrid algorithm for rainfall-runoff process modelling based on the wavelet transform and genetic fuzzy system. *J. Hydroinformatics* 16 (5), 1004–1024.
- Opolot, E. (2013). Application of remote sensing and geographical information systems in flood management: a review.
- Panagoulia, D., Dimou, G., 1997. Sensitivity of flood events to global climate change. *J. Hydrol.* 191 (1-4), 208–222.
- Panda, P.K., Sahoo, S., 2015. Modelling of floodplain using recent technology. *Eur. J. Adv. Eng. Technol.* 2 (7), 23–28.
- Petersen, M.S., 2001. Impacts of flash floods. In *Coping with flash floods*. Springer Netherlands, Dordrecht, pp. 11–13.
- Pradhan, B., 2009. Groundwater potential zonation for basaltic watersheds using satellite remote sensing data and GIS techniques. *Cent. Eur. J. Geosci.* 1, 120–129.
- Rajkhowa, S., Sarma, J., 2021. Climate change and flood risk, global climate change. In *Global climate change*. Elsevier, pp. 321–339.
- Rojas, R., Feyen, L., Bianchi, A., Dosio, A., 2012. Assessment of future flood hazard in Europe using a large ensemble of bias-corrected regional climate simulations. *J. Geophys. Res.: Atmospheres* 117 (D17).
- Saaty, T.L. (1980). The analytic hierarchy process: planning, priority setting, resource allocation.
- Sarkar, D., Mondal, P., 2020. Flood vulnerability mapping using frequency ratio (FR) model: a case study on Kulik river basin, Indo-Bangladesh Barind region. *Appl. Water Sci.* 10 (1), 1–13.
- Shen, L., Li, C., 2010. Water body extraction from Landsat ETM+ imagery using adaboost algorithm (June). In 2010 18th International Conference on Geoinformatics. IEEE, pp. 1–4 (June).
- Skilodimou, H.D., Bathrellos, G.D., Alexakis, D.E., 2021. Flood hazard assessment mapping in burned and urban areas. *Sustainability* 13 (8), 4455.
- Smiley, S.L., Hambati, H., 2019. Impacts of flooding on drinking water access in Dar es Salaam, Tanzania: implications for the Sustainable Development Goals. *J. Water, Sanit. Hyg. Dev.* 9 (2), 392–396.
- Tehrany, M.S., Pradhan, B., Jebur, M.N., 2014. Flood susceptibility mapping using a novel ensemble weights-of-evidence and support vector machine models in GIS. *J. Hydrol.* 512, 332–343.
- Tehrany, M.S., Pradhan, B., Mansor, S., Ahmad, N., 2015. Flood susceptibility assessment using a GIS-based support vector machine model with different kernel types. *Catena* 125, 91–101.
- Himanshu Thakkar (2019, August 31). Unprecedented Dam flood situation in Uttara Kannada in Aug 2019 Retrieved from (<https://sandrp.in/2019/08/31/unprecedented-dam-flood-situation-in-uttara-kannada-in-aug-2019/>).
- The New Indian Express. (2019, August 06). Karnataka rains: Over 100 flood-hit families shifted to rehab centres in Uttara Kannada Retrieved from (<https://www.newindianexpress.com/states/karnataka/2019/Aug/06/karnataka-rains-over-100-flood-hit-families-shifted-to-rehab-centres-in-uttara-kannada-2015057.html>).
- Vilasan, R.T., Kapse, V.S., 2022. Evaluation of the prediction capability of AHP and F-AHP methods in flood susceptibility mapping of Ernakulam district (India). *Nat. Hazards* 112 (2), 1767–1793.
- Zaharia, L., Costache, R., Prăvălie, R., Ioana-Toroimac, G., 2017. Mapping flood and flooding potential indices: a methodological approach to identifying areas susceptible to flood and flooding risk. Case study: the Prahova catchment (Romania). *Front. Earth Sci.* 11, 229–247.
- Zou, K.H., O'Malley, A.J., Mauri, L., 2007. Receiver-operating characteristic analysis for evaluating diagnostic tests and predictive models. *Circulation* 115 (5), 654–657.